

## Article

# Ionic Conductivity of Hybrid Composite Solid Polymer Electrolytes of $\text{PEO}_n\text{LiClO}_4$ -Cubic $\text{Li}_7\text{La}_3\text{Zr}_2\text{O}_{12}$ Films

Parisa Bashiri <sup>1</sup>, T. Prasad Rao <sup>1</sup>, Gholam-Abbas Nazri <sup>1</sup>, Ratna Naik <sup>1</sup> and Vaman M. Naik <sup>2,\*</sup>

<sup>1</sup> Department of Physics and Astronomy, Wayne State University, Detroit, MI 48202, USA; parisaphys94@yahoo.com (P.B.); prasadphd2011@gmail.com (T.P.R.); nazri@wayne.edu (G.-A.N.); rnaik@wayne.edu (R.N.)

<sup>2</sup> Department of Natural Sciences, University of Michigan-Dearborn, Dearborn, MI 48128, USA

\* Correspondence: vmnaik@umich.edu

**Abstract:** Ionic conductivity of the polyethylene oxide- $\text{LiClO}_4$  ( $\text{PEO}_n\text{LiClO}_4$ ) solid polymer electrolyte (SPE) films with an EO:Li ratio ( $n$ ) of 10, 12, 15, as well as the hybrid composite solid polymer electrolyte (CSPE) films of  $\text{PEO}_n\text{LiClO}_4$  containing 50 wt% of cubic- $\text{Li}_7\text{La}_3\text{Zr}_2\text{O}_{12}$  (LLZO) sub-micron sized particles, have been studied by varying Li-salt content in the films. The complex AC dielectric permittivity and conductivity data obtained from electrical impedance measurements were fitted using a generalized power-law, including the effects of electrode polarization applied at low AC frequencies to obtain various relaxation times. In addition to increased mechanical and thermal robustness, the CSPE films show higher values of ionic conductivity,  $>10^{-4}$  S/cm at room temperature compared to those of SPE films with  $n = 12$  and 15. On the contrary, the ionic conductivity of CSPE with  $n = 10$  decreases by a factor of three compared to the corresponding SPE film due to increased polymer structural reorientation and Li-ion pairing effects. The Vogel–Tammann–Fulcher behavior of the temperature-dependent conductivity data indicates a close correlation between the ionic conductivity and polymer segmental relaxation. The  $\text{PEO}_{12}\text{LiClO}_4$ -LLZO film shows the lowest activation energy of  $\sim 0.05$  eV.

**Keywords:** ionic conductivity; cubic  $\text{Li}_7\text{La}_3\text{Zr}_2\text{O}_{12}$ ; composite solid polymer electrolytes



**Citation:** Bashiri, P.; Rao, T.P.; Nazri, G.-A.; Naik, R.; Naik, V.M. Ionic Conductivity of Hybrid Composite Solid Polymer Electrolytes of  $\text{PEO}_n\text{LiClO}_4$ -Cubic  $\text{Li}_7\text{La}_3\text{Zr}_2\text{O}_{12}$  Films. *Processes* **2021**, *9*, 2090. <https://doi.org/10.3390/pr9112090>

Academic Editor: Yanbao Fu

Received: 26 October 2021

Accepted: 18 November 2021

Published: 22 November 2021

**Publisher's Note:** MDPI stays neutral with regard to jurisdictional claims in published maps and institutional affiliations.



**Copyright:** © 2021 by the authors. Licensee MDPI, Basel, Switzerland. This article is an open access article distributed under the terms and conditions of the Creative Commons Attribution (CC BY) license (<https://creativecommons.org/licenses/by/4.0/>).

## 1. Introduction

Li-ion conducting polymer electrolyte films have attracted much interest over the years because of their applications in all-solid-state Li-ion batteries and other energy storage/generating devices [1,2]. A solid polymer electrolyte (SPE), consisting of dissolved Li-salts in polymers, and a composite solid polymer electrolyte (CSPE) mixed with either inorganic oxide fillers or solid inorganic electrolytes are considered promising replacements for organic liquid-based electrolytes [3–6]. Research has shown that the ionic conductivity of SPE films is promoted by coupled motion of Li-ions and polymer segments in amorphous polymer regions [7,8], hence plasticizers are added to increase the fraction of amorphous regions, but adversely affect the mechanical and thermal stability of SPE films [4–6,9]. There have been several studies which have shown that the addition of inorganic fillers such as  $\text{TiO}_2$ ,  $\text{SiO}_2$ ,  $\text{Al}_2\text{O}_3$ ,  $\text{ZrO}_2$ ,  $\text{BaTiO}_3$  to a plasticized host polymer electrolyte enhances the ionic conductivity while maintaining good physical properties [4,10–13]. CSPE films with high ionic conductivity ( $>10^{-4}$  S  $\text{cm}^{-1}$ ), negligible electronic conductivity, good mechanical stability, and good electrochemical properties are desired for applications [4–6].

Recently, hybrid CSPE films of polyethylene oxide (PEO) complexed with  $\text{LiClO}_4$  and filled with sub-micron to micron-sized garnet  $\text{Li}_7\text{La}_3\text{Zr}_2\text{O}_{12}$  (LLZO) particles have been intensely studied [14–17]. LLZO is an inorganic garnet-type material that occurs in both tetragonal and cubic crystalline phases, but cubic LLZO is stabilized by doping with Al [18–20]. The tetragonal phase of LLZO is stable, but shows a room temperature conductivity ( $2 \times 10^{-6}$  S  $\text{cm}^{-1}$ ) that is two orders of magnitude lower than that of the

cubic LLZO [18]. Cubic LLZO shows good ionic conductivity ( $>2 \times 10^{-4} \text{ S cm}^{-1}$  at  $25^\circ\text{C}$ ), chemical stability, and a wide electrochemical voltage window [21,22]. Zheng et al. have employed Li NMR to probe the Li-ion diffusion pathway within cubic LLZO-PEO-LiClO<sub>4</sub> composite electrolytes in a symmetric Li-battery cell to show that Li-ions mainly pass through LLZO ceramic particles [14]. Furthermore, a flexible PEO-Li salt-based membrane consisting of a 3D ion-conducting network of LLZO nanofibers has been shown to effectively block a dendrite formation in a symmetric Li-electrolyte-Li cell [23].

A recent study with tetragonal LLZO as a filler in PEO<sub>15</sub>LiClO<sub>4</sub> (PEO Mw =  $6 \times 10^6$ ) showed that the addition of sub-micron sized LLZO particles increases the conductivity, reaching a maximum value of  $10^{-5} \text{ S cm}^{-1}$  at  $35^\circ\text{C}$  for PEO films with 52.5 wt% LLZO [15]. On the other hand, a study with cubic-LLZO micron-sized particles as a filler in PEO<sub>20</sub>LiClO<sub>4</sub> (PEO Mw =  $10^5$ ) showed a decrease in conductivity of the composite films with the addition of 30–50 vol% of LLZO [16]. We investigated the AC conductivity of PEO<sub>15</sub>LiClO<sub>4</sub> (PEO Mw =  $10^6$ ) films containing 50 wt% of cubic-LLZO particles [17]. We observed an enhancement in conductivity ( $1.4 \times 10^{-4} \text{ S cm}^{-1}$  at  $30^\circ\text{C}$ ) by two orders of magnitude, compared to that of PEO<sub>15</sub>LiClO<sub>4</sub> films. Recently, Chen et al. have reported Li-ion conductivity  $>10^{-4} \text{ S cm}^{-1}$  at  $30^\circ\text{C}$  for the composite solid electrolyte of PEO<sub>8</sub>LiTFSI (PEO Mw =  $6 \times 10^5$ ) containing 10 wt% of garnet Li<sub>6.4</sub>La<sub>3</sub>Zr<sub>1.4</sub>Ta<sub>0.6</sub>O<sub>12</sub> (LLZTO) micron-sized particles [24]. Further increase in wt% of LLZTO in the composite electrolytes resulted in a decrease in Li-ion conductivity. However, their measurements on “Polymer in Ceramics” films with 80 wt% LLZTO showed that the ionic conductivity depends on the amount of LiTFSI added to the composite.

In the present work, we have investigated the effect of the Li-salt content (EO:Li ratio  $n = 10, 12, 15$ ) on the AC conductivity of PEO<sub>*n*</sub>LiClO<sub>4</sub>—50 wt% cubic LLZO hybrid CSPE films as well as SPE films of PEO<sub>*n*</sub>LiClO<sub>4</sub>. We have used a comprehensive and complex dielectric function that includes ionic, segmental, and dipolar relaxation times to explain the observed dielectric permittivity and AC conductivity data rather than using simple empirical equivalent circuits which do not explain the electrode polarization at low applied AC frequencies. In addition to enhanced mechanical and thermal robustness, the CSPE films show higher values of ionic conductivity  $>10^{-4} \text{ S cm}^{-1}$  ( $30^\circ\text{C}$ ) compared to those of SPE films at lower Li-ion concentration ( $n = 12$  and  $15$ ). The analyses of temperature-dependent conductivity showed Vogel–Tammann–Fulcher (VTF) behavior, indicating a close correlation between ionic conductivity and segmental relaxation with a lower activation energy in CSPE compared to SPE. However, the ionic conductivity of CSPE decreases at a higher Li-ion concentration ( $n = 10$ ), roughly by a factor of three compared to SPE. We associate this observation with structural reorientation of the PEO matrix and Li-ion aggregation effects in the presence of LLZO particles.

## 2. Materials and Methods

About 100 μm thickness ( $t$ ) films of PEO<sub>*n*</sub>LiClO<sub>4</sub> and PEO<sub>*n*</sub>LiClO<sub>4</sub>-LLZO with  $n = 10, 12$  and  $15$  were prepared as described in detail elsewhere [17]. All films were desiccated for a day before making structural and electrochemical measurements. Infrared and Raman spectra of the films showed no solvent characteristic bands implying the absence of residual solvent in the films. Structural characterization (X-ray diffraction and scanning electron microscopy), thermal stability, and electrical impedance of the films in the 1 Hz to 300 kHz range were carried out as described in [17].

The complex permittivity,  $\epsilon^* = \epsilon' - i\epsilon''$ , and AC conductivity,  $\sigma^* = \sigma' + i\sigma''$ , were calculated using the measured real and imaginary parts of the impedance ( $Z^* = Z' + iZ''$ ) from the following relations,

$$\epsilon' = \frac{t}{\omega A \epsilon_0} \frac{Z''}{Z'^2 + Z''^2} \quad (1)$$

$$\epsilon'' = \frac{t}{\omega A \epsilon_0} \frac{Z'}{Z'^2 + Z''^2} \quad (2)$$

$$\sigma^* = i\varepsilon_0\omega\varepsilon^* = i\varepsilon_0\omega(\varepsilon' - i\varepsilon'') \quad (3)$$

where  $A$  is the area of the blocking electrode. Calculated real and imaginary parts of conductivity were fitted to the following generalized expression for the AC conductivity in ion-conducting materials [25,26].

$$\sigma^*(\omega) = \sigma_{dc} - \frac{\sigma_{dc} - \sigma_o}{1 + (i\omega/\omega_j)^\alpha} + i\omega\varepsilon_0 \frac{\Delta\varepsilon}{(1 + (i\omega/\omega_R)^\beta)^\gamma} \quad (4)$$

The above equation accounts for the electrode polarization and the relaxation processes that occur in ion-conducting polymeric materials. In Equation (4),  $\sigma_{dc}$  is the frequency-independent DC conductivity,  $\sigma_o$  is a pre-factor used in describing the AC conductivity in the region not affected by electrode polarization,  $\omega_j$  is the frequency corresponding to the full development of electrode polarization which is also the peak frequency,  $f_{peak,\sigma''}$  in the  $\sigma''$  vs.  $f$  plot,  $\omega_R$  is the characteristic frequency of the dipole relaxation,  $\Delta\varepsilon = \varepsilon_s - \varepsilon_\infty$  is the difference between static and high frequency limit of dielectric constant,  $\omega$  is the angular frequency of the applied AC electric field, and  $\alpha$ ,  $\beta$  and  $\gamma$  are  $<1$ .

### 3. Results and Discussion

The XRD patterns of  $PEO_nLiClO_4$ , and  $PEO_nLiClO_4$ -LLZO films are shown in Figure 1. Two strong characteristic peaks of crystalline PEO riding on a broad background are seen in the XRD patterns, confirming the semi-crystalline nature of the polymer. Figure 1a shows the region containing the (120) and (112) peaks of PEO occurring at  $2\theta = 19.2^\circ$  and  $23.5^\circ$ . PEO has a monoclinic crystalline structure with cell parameters:  $a = 0.796$  nm,  $b = 1.311$  nm,  $c = 1.930$  nm, and  $\beta = 124.8^\circ$  [27]. The diffraction peak profile from  $2\theta = 23\text{--}24^\circ$  is actually a composite of (112), (032),  $(\bar{1}32)$ ,  $(\bar{2}12)$  and  $(\bar{2}02)$  peaks. We can assign a small peak seen at  $2\theta \approx 22.2^\circ$  to the (121) peak of PEO. As the Li-ion concentration in the composite film increases, the fraction of the amorphous phase of the polymer increases leading to an increase in intensity of the broad background in the entire diffractogram from  $2\theta = 10^\circ$  to  $80^\circ$  (not shown here), while PEO crystalline peaks show a relative decrease in intensity. Polymer electrolytes acquire local relaxation and segmental motion of solvent polymer chains to facilitate Li-ion motion through the amorphous phase, thus increasing the ionic conductivity. The broadening of the background peak is clearly seen in Figure 1a for SPE films without LLZO particles. The XRD patterns of CSPE films with LLZO particles are dominated by the diffraction peaks arising from crystalline cubic-LLZO. Figure 1b shows the XRD patterns of  $PEO_nLiClO_4$ -LLZO with a different Li-ion concentration. The cubic-LLZO peaks are indicated by the asterisks. It should be noted that the most intense peak of LLZO overlaps with the (120) peak of PEO, while the peak at  $2\theta \approx 23.2^\circ$  coincides with (112) peak of PEO. Significant changes are seen in the XRD pattern of  $PEO_{10}LiClO_4$ -LLZO (top panel of Figure 1b) where the peak at  $2\theta \approx 21.8^\circ$  has become somewhat intense, indicating structural reorientation of the PEO-Li matrix in the presence of LLZO particles. It is known that internal rotational degrees of freedom about C-O and C-C single bonds along the polymer backbone can adopt different periodic helical structures depending on the environment [27,28].

All the films investigated in this work were free-standing and mechanically robust, especially CSPE films with LLZO. As shown in our earlier work, the CSPE films retain their mechanical integrity at high temperatures up to  $120^\circ\text{C}$  [17]. Figure 2 shows the SEM images of  $PEO_nLiClO_4$  and  $PEO_nLiClO_4$ -LLZO films with different Li-salt content. Films with low Li-salt content ( $n = 15$ ) show large, nearly spherical-shaped PEO spherulites containing crystalline PEO with a rough surface morphology. As the Li-salt content of the films increases, there is a significant change in film morphology due to the disappearance of large spherulites, indicating increased amorphous regions as confirmed by XRD results. The investigation of crystallization in a high salt PEO-salt polymer electrolyte using optical microscopy and differential scanning calorimetry has shown non-volume filling spherulites with increased amorphous regions, leading to a broad melting transition [29]. Figure 2b

shows the SEM images of corresponding  $\text{PEO}_n\text{LiClO}_4\text{-LLZO}$  films. A drastic reduction in the granular size is seen in  $\text{PEO}_{15}\text{LiClO}_4\text{-LLZO}$  film compared to  $\text{PEO}_{15}\text{LiClO}_4$ . LLZO particles may act as nucleating sites for the growth of a large number of smaller PEO spherulites as seen in an earlier study with a different filler [30]. In general, the addition of LLZO particles makes  $\text{PEO}_n\text{LiClO}_4\text{-LLZO}$  film morphology smoother compared to  $\text{PEO}_n\text{LiClO}_4$ .

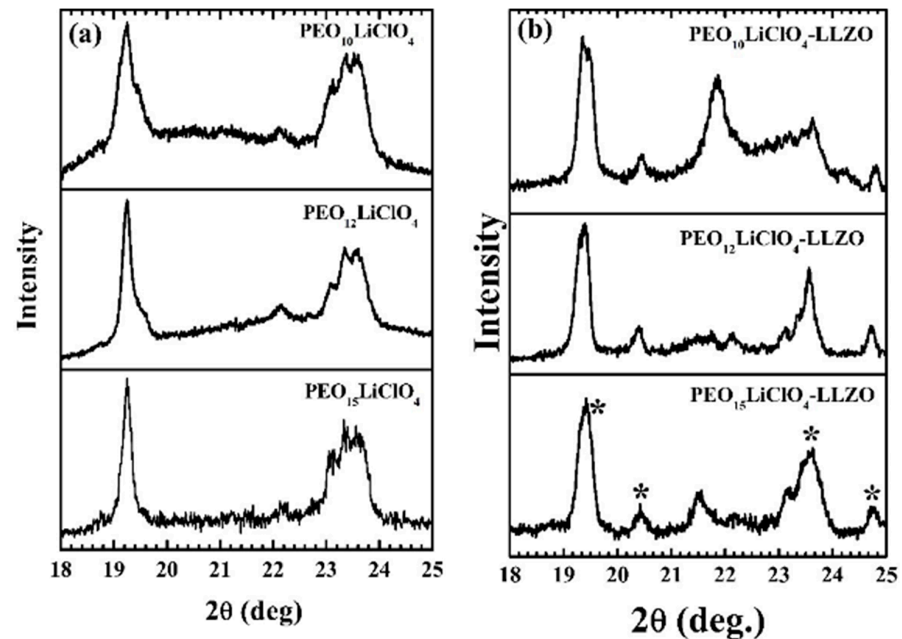


**Figure 1.** (a) XRD patterns of  $\text{PEO}_n\text{LiClO}_4$  and (b) XRD patterns of  $\text{PEO}_n\text{LiClO}_4\text{-LLZO}$ . LLZO peaks are marked with asterisks.

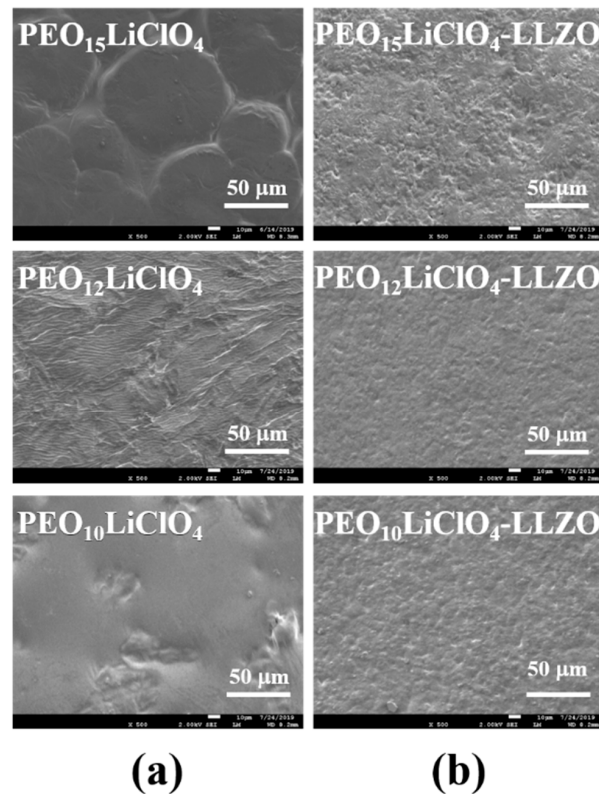


**Figure 2.** Scanning electron micrographs of (a)  $\text{PEO}_n\text{LiClO}_4$  and (b)  $\text{PEO}_n\text{LiClO}_4\text{-LLZO}$  films.

Figures 3 and 4 show the dielectric permittivity and loss tangent ( $\tan \delta = \epsilon''/\epsilon'$ ) of  $\text{PEO}_n\text{LiClO}_4$  and  $\text{PEO}_n\text{LiClO}_4\text{-LLZO}$  films at 30 °C as a function of frequency.  $\epsilon'$  and  $\epsilon''$  show the typical frequency dependence of ion-conducting materials. The observed values of  $\epsilon'$  and  $\epsilon''$  at low frequencies are four to six orders of magnitude higher than their limiting (high frequency) values due to electrode polarization [25]. At low frequencies of the applied AC field, ions traverse long distances and accumulate on the blocking electrodes, forming an electrical double layer capacitance leading to large dielectric permittivity. As the frequency is lowered from the high-frequency region,  $\epsilon'$  begins to rise steeply due to the onset of electrode polarization, reaching a full development at about 100 Hz to 1 kHz for the samples. The peak in the loss tangent spectrum (Figure 4) is associated with polymer chain segmental relaxation time,  $\tau_s$ , and it is calculated using the relation  $\tau_s = 1/2\pi f_p$ , where  $f_p$  is the frequency corresponding to the peak in the loss tangent spectrum [17]. The frequency,  $f_j$ , at which the full electrode polarization occurs, is related to the ionic relaxation time and corresponds to the peak in the  $\sigma''$  spectrum (Figure 5). The ionic relaxation time,  $\tau_j$ , is related to  $f_j$  via  $\tau_j = 1/2\pi f_j$  [17]. The experimental  $\epsilon'$  and  $\epsilon''$ , and  $\tan \delta$  data shown in Figures 3 and 4 are fitted using Equations (1) and (2) and the fitted data are shown as solid lines. The real and imaginary parts of conductivity data,  $\sigma'$  and  $\sigma''$ , shown in Figure 5 are fitted using Equation (4). Table 1 summarizes the best fit parameters  $\Delta\epsilon$ ,  $\sigma_{dc}$ ,  $\tau_j$ ,  $\tau_s$ ,  $\tau_R$ ,  $\alpha$ ,  $\beta$  and  $\gamma$  for the  $\text{PEO}_n\text{LiClO}_4$  and  $\text{PEO}_n\text{LiClO}_4\text{-LLZO}$  films, where  $\tau_R = 1/\omega_R$  is the EO-dipole relaxation time.

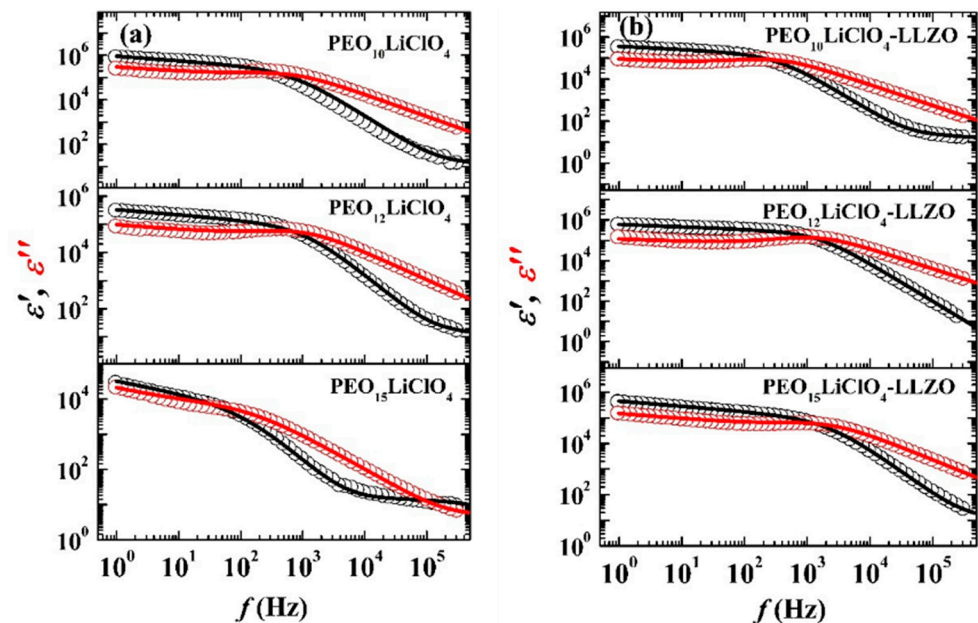
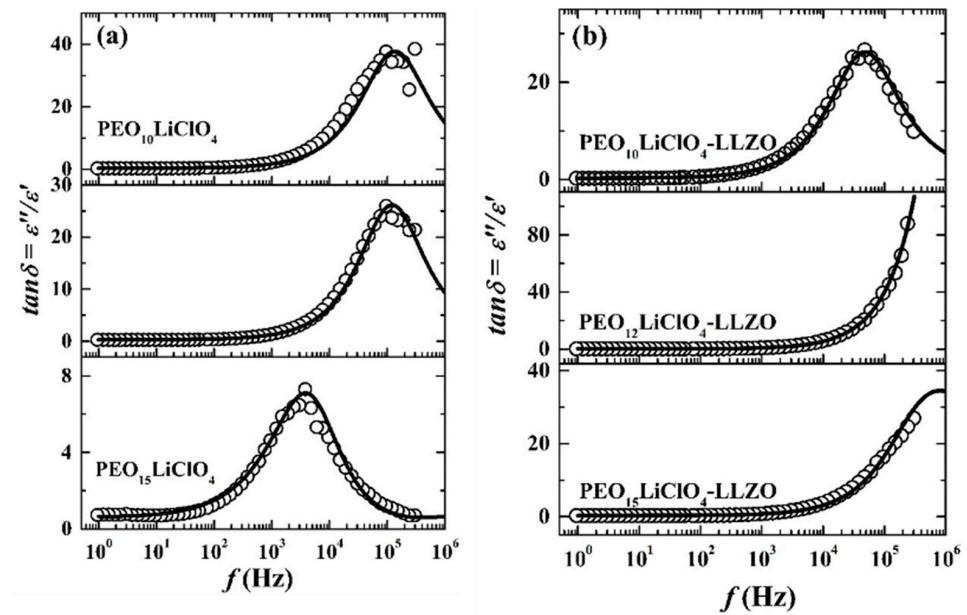
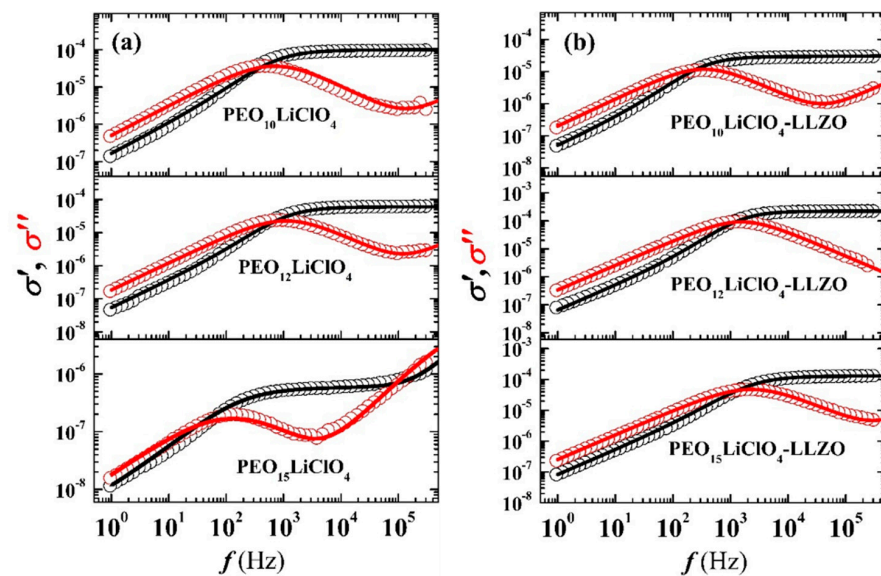


Figure 3. Frequency dependence of  $\epsilon'$  and  $\epsilon''$  of (a)  $\text{PEO}_n\text{LiClO}_4$  and (b)  $\text{PEO}_n\text{LiClO}_4\text{-LLZO}$ . The open circles and solid lines represent the experimental data and the fitted data.



**Figure 4.** (a) Loss tangent of  $\text{PEO}_n\text{LiClO}_4$  and (b)  $\text{PEO}_n\text{LiClO}_4\text{-LLZO}$  films. The open circles and solid lines represent the experimental data and the fitted data.



**Figure 5.** The frequency dependence of  $\sigma'$  and  $\sigma''$  of (a)  $\text{PEO}_n\text{LiClO}_4$  and (b)  $\text{PEO}_n\text{LiClO}_4\text{-LLZO}$  films. The open circles and solid lines represent the experimental data and the fitted data.

**Table 1.** The ionic ( $\tau_j$ ) and segmental ( $\tau_s$ ) relaxation times, and other parameters obtained from fitting the complex dielectric permittivity and conductivity of  $\text{PEO}_n\text{LiClO}_4$  and  $\text{PEO}_n\text{LiClO}_4\text{-LLZO}$  at 30 °C.

Sample	$\Delta\epsilon$	$\sigma_{dc}$ ( $\text{S cm}^{-1}$ )	$\tau_j$ (ms)	$\tau_s$ ( $\mu\text{s}$ )	$\tau_R$ ( $\mu\text{s}$ )	$\alpha$	$\beta$	$\gamma$	$\tau_s/\tau_j$
$\text{PEO}_{15}\text{LiClO}_4$	15	$5.8 \times 10^{-7}$	1.22	38.8	0.35	0.68	0.65	1.0	0.032
$\text{PEO}_{12}\text{LiClO}_4$	18	$6.0 \times 10^{-5}$	0.15	1.38	0.32	0.82	0.60	1.0	0.009
$\text{PEO}_{10}\text{LiClO}_4$	20	$9.5 \times 10^{-5}$	0.11	1.33	0.29	0.84	0.53	1.0	0.012
$\text{PEO}_{15}\text{LiClO}_4\text{-LLZO}$	15	$1.4 \times 10^{-4}$	0.06	0.28	0.24	0.80	0.65	1.0	0.005
$\text{PEO}_{12}\text{LiClO}_4\text{-LLZO}$	20	$2.2 \times 10^{-4}$	0.05	0.12	0.04	0.88	0.70	0.65	0.002
$\text{PEO}_{10}\text{LiClO}_4\text{-LLZO}$	24	$3.0 \times 10^{-5}$	0.45	3.30	0.40	0.85	0.60	0.65	0.007

The ionic conductivity of  $\text{PEO}_n\text{LiClO}_4$  film strongly depends on its Li-salt content (see Table 1). Although the number of Li-ions increases with salt content, their mobility is affected by the progressive occurrence of ion-pairing effects [31]. It is interesting to note that the ionic conductivity increases by two orders of magnitude when salt content is increased from  $n = 15$  to  $n = 12$ , but does not change significantly upon further increase from  $n = 12$  to  $n = 10$ . FTIR studies of PEO with  $\text{LiClO}_4$  salt (90:10) have demonstrated the formation of ion pairs, as indicated by the presence of a shoulder peak ( $\sim 635 \text{ cm}^{-1}$ ) of the main band of  $623 \text{ cm}^{-1}$  corresponding to the free  $\text{ClO}_4^-$  anion [32,33]. Li-ion pairing thus limits the maximum obtainable ionic conductivity in  $\text{PEO}_n\text{LiClO}_4$  by increasing salt content alone. As observed in numerous other CSPE containing inorganic fillers, inclusion of 50 wt% LLZO particles in  $\text{PEO}_n\text{LiClO}_4$  not only enhances film mechanical robustness and thermal stability, but also increases ionic conductivity by more than two orders of magnitude in CSPE with  $n = 15$ , and a factor of four with  $n = 12$ . We associate this increase to smoother film morphology (see Figure 2) in CSPE due to the formation of a large number of smaller-sized PEO spherulites, thus increasing the ratio of amorphous to crystalline PEO [30,34]. On the other hand, the ionic conductivity CSPE with  $n = 10$  decreases by a factor of three compared to corresponding SPE film due to increased polymer structural reorientation (see top panel of Figure 1b). It is also interesting to note that  $\text{PEO}_{10}\text{LiClO}_4$ -LLZO seems to contain slightly larger spherulites compared to  $\text{PEO}_{12}\text{LiClO}_4$ -LLZO (see Figure 2b). This could be due to increased ion-pairing effects which are known to occur at high salt concentrations [31,32].

The presence of a single peak in the spectrum of  $\tan \delta$  (Figure 4a, b) confirms the Li-ion-dipolar coupled cooperative segmental motion of PEO macromolecules in these electrolytes [35]. In Figure 4a, the peak shifts to a higher frequency in both  $\text{PEO}_{10}\text{LiClO}_4$  and  $\text{PEO}_{12}\text{LiClO}_4$  films compared to  $\text{PEO}_{15}\text{LiClO}_4$ . As the Li-salt increases in  $\text{PEO}_n\text{LiClO}_4$ ,  $\tau_s$  and  $\tau_j$  values are reduced significantly, reaching limiting values around  $n = 10$ . As explained earlier, further increase in salt content ( $n = 10$ ) resulted in the slowing of both ion and polymer segmental motions due to ion-pairing effects. However, CSPE films of  $\text{PEO}_n\text{LiClO}_4$ -LLZO with  $n = 15$  and 12 show even further reduction in  $\tau_s$  by a factor two, and  $\tau_j$  by a factor of four. The ionic and segmental relaxation times listed in Table 1 clearly show an intimate coupling between ionic conductivity and segmental motion. The ratio  $\tau_s/\tau_j$ , called the decoupling ratio, of less than one is indicative of a strong coupling [36–38]. The decoupling ratios for all the composite films studied in this work are in the range of 0.002 to 0.032 (Table 1) implying a strong coupling between ionic conductivity and segmental motion, i.e., the ionic motion is facilitated by the polymer segmental motion. The observed value of ionic conductivity of  $2.2 \times 10^{-4} \text{ S cm}^{-1}$  in  $\text{PEO}_{12}\text{LiClO}_4$ -LLZO is the highest among all the composite films studied in this work. This is higher than the conductivity reported for  $\text{PEO}_{15}\text{LiClO}_4$ -tetragonal-LLZO [15] and  $\text{PEO}_{15}\text{LiClO}_4$ -cubic-LLZO [16].

To investigate the nature of the ion-conduction process in these composite films, we have studied the temperature dependence of ionic conductivity. The shifting of peak frequency to higher values of  $\tan \delta$  with increasing temperature is an indication of a thermally activated conduction process, and the temperature dependence of conductivity does not follow Arrhenius law [31]. Many polymer electrolytes exhibit Non-Arrhenius temperature dependence of conductivity due to the coupling of ionic motion and polymer segmental dynamics. Such temperature dependence of conductivity is often described by an empirical equation [39–42]. We have analyzed the measured temperature dependence of conductivity data using the VTF equation [17],

$$\sigma = Ae^{-E_a/k_B(T-T_0)} \quad (5)$$

where  $A$  is a constant related to the number of charge carriers.  $E_a$  is the activation energy barrier for Li-ion motion, and  $T_0$  is the ideal glass transition temperature. In general, the observed value of glass transition temperature  $T_g > T_0$  is where the polymer becomes

macroscopically rubbery rather than glassy. The excess thermal energy,  $k_B (T - T_g)$ , provides the mobility to the polymer chain segments.

Figure 6 shows the conductivity versus reciprocal of temperature for  $\text{PEO}_n\text{LiClO}_4$  and  $\text{PEO}_n\text{LLZO-LiClO}_4$  films. The solid lines in Figure 6 represent the fitted data using Equation (5), and the excellent fits obtained indicate the temperature dependence of conductivity, and is described by the VTF equation implying a coupled motion of Li-ions with the polymer segmental motion. Table 2 shows the activation energy and the  $T_o$  for  $\text{PEO}_n\text{LiClO}_4$  and  $\text{PEO}_n\text{LLZO-LiClO}_4$  films using the VTF equation. In ceramic-free films, the activation energy of  $\text{PEO}_{15}\text{LiClO}_4$  is 0.32 eV and decreases by more than a factor of three with increasing the Li-salt content. For CSPE films of  $\text{PEO}_n\text{LiClO}_4\text{-LLZO}$  with  $n = 12$  and 15, the activation energy decreases nearly by a factor of five.  $T_o$  values of 50 K–80 K below the glass transition temperature ( $T_g \approx 245$  K) are in agreement with the values observed for other PEO-based electrolytes [39–42].

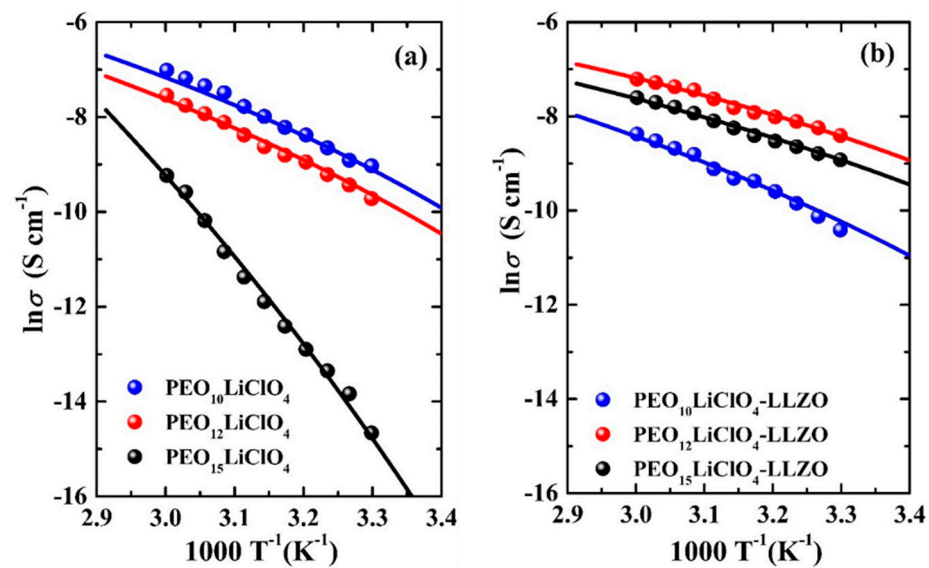


**Figure 6.** Ionic conductivity vs.  $1000 T^{-1}$  for (a)  $\text{PEO}_n\text{-LiClO}_4$  and (b)  $\text{PEO}_n\text{LiClO}_4\text{-LLZO}$  films. Filled circles represent the experimental data and the solid lines represent the VTF fit.

**Table 2.** Activation energy and  $T_o$  of  $\text{PEO}_n\text{LiClO}_4$  and  $\text{PEO}_n\text{LiClO}_4\text{-LLZO}$  obtained fitting the temperature-dependent ionic conductivity with VTF model.

Sample	$E_a$ (eV)	$T_o$ (K)
$\text{PEO}_{15}\text{LiClO}_4$	0.32	175
$\text{PEO}_{12}\text{LiClO}_4$	0.09	192
$\text{PEO}_{10}\text{LiClO}_4$	0.09	197
$\text{PEO}_{15}\text{LiClO}_4\text{-LLZO}$	0.07	185
$\text{PEO}_{12}\text{LiClO}_4\text{-LLZO}$	0.05	198
$\text{PEO}_{10}\text{LiClO}_4\text{-LLZO}$	0.09	185

#### 4. Conclusions

We have studied the effect of Li-salt content on the ionic conductivity of SPE films of  $\text{PEO}_n\text{LiClO}_4$  and CSPE films of  $\text{PEO}_n\text{LiClO}_4\text{-LLZO}$  containing 50 wt% sub-micron sized cubic  $\text{Li}_7\text{La}_3\text{Zr}_2\text{O}_{12}$  (LLZO) particles, with  $n = 10, 12$ , and 15. Ionic and polymer relaxation times obtained from the fitting of the complex permittivity and conductivity data to a generalized power-law indicate a strong coupling between ionic conductivity and segmental motion, and the ionic motion is facilitated by the polymer segmental motion. In ceramic-free  $\text{PEO}_n\text{LiClO}_4$  films, the ionic conductivity increases by two orders of magnitude when Li-salt content is increased ( $n = 15$  to  $n = 12$ ) and does not change significantly upon

further increase of Li-salt content ( $n = 12$  to  $n = 10$ ). On the other hand, the addition of 50 wt% LLZO particles not only enhances film mechanical robustness and thermal stability, but also increases ionic conductivity by more than two orders of magnitude in CSPE films with  $n = 15$  due to the formation of a large number of smaller sized PEO spherulites. The  $\text{PEO}_n\text{LiClO}_4\text{-LLZO}$  CSPE film with  $n = 12$  appears to yield the optimum ionic conductivity of  $2.2 \times 10^{-4} \text{ S cm}^{-1}$  at  $30^\circ\text{C}$ , and further increase in Li-loading resulted in a decrease in conductivity due to the polymer recrystallization and ion-pairing effects. The temperature-dependent ionic conductivity follows the Vogel–Tammann–Fulcher behavior, suggesting a thermally activated conduction process, and the activation energy decreases from 0.35 eV in  $\text{PEO}_{15}\text{LiClO}_4$  SPE film to 0.05 eV in  $\text{PEO}_{12}\text{LiClO}_4\text{-LLZO}$  CSPE film. With further adjustments in Li-salt content and LLZO concentration, it may be possible to improve the ionic conductivity to achieve a higher value desired for applications.

**Author Contributions:** Conceptualization, R.N., V.M.N. and G.-A.N.; methodology, P.B., T.P.R.; software, P.B., V.M.N.; validation, R.N., V.M.N., G.-A.N.; formal analysis, P.B., T.P.R.; investigation, P.B., T.P.R.; resources, R.N.; data curation, P.B., T.P.R.; writing—original draft preparation, V.M.N.; writing—review and editing, R.N., V.M.N.; visualization, R.N., V.M.N.; supervision, R.N.; project administration, R.N.; funding acquisition, R.N. All authors have read and agreed to the published version of the manuscript.

**Funding:** This research is supported by the College of Liberal Arts and Sciences, Wayne State University.

**Institutional Review Board Statement:** Not applicable.

**Informed Consent Statement:** Not applicable.

**Conflicts of Interest:** The authors declare that they have no competing interest.

## References

1. Goodenough, B.; Kim, Y. Challenges for rechargeable Li batteries. *Chem. Mater.* **2010**, *22*, 587–603. [[CrossRef](#)]
2. Tarascon, J.M.; Armand, M. Issues and challenges facing rechargeable lithium batteries. *Nature* **2001**, *414*, 359–367. [[CrossRef](#)] [[PubMed](#)]
3. Agrawal, R.C.; Pandey, G.P. Solid Polymer electrolytes: Materials designing and all-solid-state-battery applications: An overview. *J. Phys. D Appl. Phys.* **2008**, *41*, 223001. [[CrossRef](#)]
4. Yue, L.; Ma, J.; Zhang, J.; Zhao, J.; Dong, S.; Liu, Z. All solid-state polymer electrolytes for high-performance lithium ion batteries. *Energy Storage Mater.* **2016**, *5*, 139–164. [[CrossRef](#)]
5. Liang, J.; Luo, J.; Sun, Q.; Yang, X.; Li, R.; Sun, X. Recent progress on solid-state hybrid electrolytes for solid-state lithium batteries. *Energy Storage Mater.* **2019**, *21*, 308–334. [[CrossRef](#)]
6. Dirican, M.; Yan, C.; Zhu, P.; Zhang, X. Composite solid electrolytes for all-solid-state lithium batteries. *Mater. Sci. Eng. R* **2019**, *136*, 27–46. [[CrossRef](#)]
7. Seki, S.; Susan, M.A.B.H.; Kaneko, T.; Tokuda, H.; Noda, A.; Watanabe, M. Distinct difference in ionic transport behavior in polymer electrolytes depending on the matrix polymers and incorporated salts. *J. Phys. Chem. B* **2005**, *109*, 3886–3892. [[CrossRef](#)]
8. Money, B.K.; Hariharan, K.; Swenson, J. Relation between structural and conductivity relaxation in PEO and PEO based electrolytes. *Solid State Ion.* **2014**, *262*, 785–789. [[CrossRef](#)]
9. Nicotera, I.; Ranieri, G.A.; Terenzi, M.; Chadwick, A.V.; Webster, M.I. A study of stability of plasticized PEO electrolytes. *Solid State Ion.* **2002**, *146*, 143–150. [[CrossRef](#)]
10. Croce, F.; Appetecchi, G.B.; Persi, L.; Scrosati, B. Nanocomposite polymer electrolytes for lithium batteries. *Nature* **1998**, *394*, 456–458. [[CrossRef](#)]
11. Pandey, G.P.; Hashmi, S.A.; Agrawal, R.C. Hot-press synthesized polyethylene oxide based proton conducting nanocomposite polymer electrolyte dispersed with  $\text{SiO}_2$  nanoparticles. *Solid State Ion.* **2008**, *179*, 543–549. [[CrossRef](#)]
12. Croce, F.; Sacchetti, S.; Scrosati, B. Advanced, lithium batteries based on high-performance composite polymer electrolytes. *J. Power Sources* **2006**, *162*, 685–689. [[CrossRef](#)]
13. Sun, H.Y.; Takeda, Y.; Imanishi, N.; Yamamoto, O.; Sohn, H.-J. Ferroelectric materials as a ceramic filler in solid composite polyethylene oxide-based electrolytes. *J. Electrochem. Soc.* **2000**, *147*, 2462–2467. [[CrossRef](#)]
14. Zheng, J.; Tang, M.; Hu, Y.Y. Lithium ion pathway within  $\text{Li}_7\text{La}_3\text{Zr}_2\text{O}_{12}$ -Polyethylene oxide composite electrolytes. *Angew. Chem. Int. Ed. Engl.* **2016**, *55*, 12538–12542. [[CrossRef](#)] [[PubMed](#)]
15. Choi, J.-H.; Lee, C.-H.; Yu, J.-H.; Doh, C.-H.; Lee, S.-M. Enhancement of ionic conductivity of composite membranes for all-solid-state lithium rechargeable batteries incorporating tetragonal  $\text{Li}_7\text{La}_3\text{Zr}_2\text{O}_{12}$  into a polyethylene oxide matrix. *J. Power Sources* **2015**, *274*, 458–463. [[CrossRef](#)]

16. Langer, F.; Bardenhagen, I.; Glenneberg, J.; Kun, R. Microstructure and temperature dependent lithium ion transport of ceramic-polymer composite electrolyte for solid-state lithium ion batteries based on garnet-type  $\text{Li}_7\text{La}_3\text{Zr}_2\text{O}_{12}$ . *Solid State Ion.* **2016**, *291*, 8–13. [[CrossRef](#)]
17. Bashiri, P.; Prasada Rao, T.; Naik, V.M.; Nazri, G.A.; Naik, R. AC conductivity studies of polyethylene oxide-garnet-type  $\text{Li}_7\text{La}_3\text{Zr}_2\text{O}_{12}$  hybrid composite solid polymer electrolyte films. *Solid State Ion.* **2019**, *343*, 115089. [[CrossRef](#)]
18. Buschmann, H.; Dolle, J.; Berendts, S.; Kuhn, A.; Bottke, P.; Wilkening, M.; Heitjans, P.; Senyshyn, A.; Ehrenberg, H.; Lotnyk, A.; et al. Structure and dynamics of the fast lithium ion conductor  $\text{Li}_7\text{La}_3\text{Zr}_2\text{O}_{12}$ . *Phys. Chem. Chem. Phys.* **2011**, *13*, 19378. [[CrossRef](#)]
19. Rangaswamy, E.; Wolfenstein, J.; Sakamoto, J. The role of Al and Li concentration on the formation of cubic garnet solid electrolyte of nominal composition  $\text{Li}_7\text{La}_3\text{Zr}_2\text{O}_{12}$ . *Solid State Ion.* **2012**, *206*, 28–32. [[CrossRef](#)]
20. Shao, C.; Liu, H.; Yu, Z.; Zheng, Z.; Sun, N.; Diao, C. Structure and ionic conductivity of cubic  $\text{Li}_7\text{La}_3\text{Zr}_2\text{O}_{12}$  solid electrolyte by chemical co-precipitation method. *Solid State Ion.* **2016**, *287*, 13–16. [[CrossRef](#)]
21. Cao, C.; Li, Z.-B.; Wang, X.-L.; Zhao, X.-B.; Han, W.-Q. Recent advances in inorganic solid electrolytes for lithium batteries. *Front. Energy Res.* **2014**, *2*, 25. [[CrossRef](#)]
22. Thangadurai, V.; Narayanan, S.; Pinzaru, D. Garnet-type solid-state fast Li ion conductors for Li batteries: Critical review. *Chem. Soc. Rev.* **2014**, *43*, 4714–4727. [[CrossRef](#)]
23. Fu, K.; Gong, Y.; Dai, J.; Gong, A.; Han, X.; Yao, Y.; Wang, C.; Wang, Y.; Chen, Y.; Yan, C.; et al. Flexible, solid-state, ion-conducting membrane with 3D garnet nanofiber networks for lithium batteries. *Proc. Natl. Acad. Sci. USA* **2016**, *113*, 7094. [[CrossRef](#)]
24. Chen, L.; Li, Y.; Li, S.-P.; Fan, L.-Z.; Nan, C.-W.; Goodenough, J.B. PEO/garnet composite electrolytes for solid state lithium batteries: From “ceramic-in-polymer” to “polymer-in-ceramic”. *Nano Energy* **2018**, *46*, 176–184. [[CrossRef](#)]
25. Khamzin, A.A.; Popov, I.I.; Nigmatullin, R.R. Correction of the power law of ac conductivity in ion-conducting materials due to the electrode polarization effect. *Phys. Rev. E* **2014**, *89*, 032303. [[CrossRef](#)]
26. Havriliak, S.; Negami, S. A complex plane analysis of  $\alpha$ -dispersions in some polymer systems. *J. Polym. Sci. Part C* **1996**, *14*, 99. [[CrossRef](#)]
27. Baltá Calleja, F.J.; Hay, I.L.; Keller, A. Diffraction effects in single crystals and spherulites of poly(ethylene oxide). *Kolloid ZU Z Polym.* **1966**, *209*, 128–135. [[CrossRef](#)]
28. Miyazawa, T.; Fukushima, K.; Ideguchi, Y. Molecular vibrations and structure of high polymers. III. Polarized infrared spectra, normal vibrations, and helical conformation of polyethylene glycol. *J. Chem. Phys.* **1962**, *37*, 2764. [[CrossRef](#)]
29. Choi, B.-K. Optical microscopy study on the crystallization in PEO-salt polymer electrolytes. *Solid State Ion.* **2004**, *168*, 123. [[CrossRef](#)]
30. Xi, J.; Qiu, X.; Zhu, W.; Tang, X. Enhanced electrochemical properties of poly(ethylene oxide)-based composite polymer electrolyte with ordered mesoporous materials for lithium polymer battery. *Micropor. Mesopor. Mater.* **2006**, *88*, 1–7. [[CrossRef](#)]
31. Armand, M.B.; Bruce, P.G.; Forsyth, M.; Scrosati, B.; Wiczcok, W. Polymer electrolytes. In *Energy Materials*; Bruce, D.W., O’Hare, D., Walton, R.I., Eds.; John Wiley & Sons: Hoboken, NJ, USA, 2011.
32. Jaipal Reddy, M.; Chu, P.P.; Subba Rao, U.V. Study of multiple interactions in mesoporous composite PEO electrolytes. *J. Power Sources* **2006**, *158*, 614–619. [[CrossRef](#)]
33. Wiczcok, W.; Raducha, D.; Zalewska, A.; Stevens, J. Effect of salt concentration on the conductivity of PEO-based composite polymeric electrolytes. *J. Phys. Chem. B* **1998**, *102*, 8725–8731. [[CrossRef](#)]
34. Karmarkar, A.; Ghosh, A. A comparison of ion transport in different polyethylene oxide-lithium salt composite electrolytes. *J. Appl. Phys.* **2010**, *107*, 104113. [[CrossRef](#)]
35. Choudhary, S.; Sengwa, R.J. Effects of different inorganic nanoparticles on the structural, dielectric and ion transportation properties of polymers blend based nanocomposite solid polymer electrolytes. *Electrochim. Acta* **2017**, *247*, 924–941. [[CrossRef](#)]
36. McLin, M.G.; Angell, C.A. Contrasting conductance/viscosity relations in liquid states of vitreous and polymer solid electrolytes. *J. Phys. Chem.* **1988**, *92*, 2083–2086. [[CrossRef](#)]
37. Angell, C.A. Mobile ions in amorphous solids. *Annu. Rev. Phys. Chem.* **1992**, *43*, 693–717. [[CrossRef](#)]
38. Ratner, M.A.; Shriver, D.F. Ion Transport in Solvent-Free Polymers. *Chem. Rev.* **1988**, *88*, 109–124. [[CrossRef](#)]
39. Pradhan, D.K.; Karan, N.K.; Thomas, R.; Katiyar, R.S. Coupling of conductivity to the relaxation process in polymer electrolytes. *Mater. Chem. Phys.* **2014**, *147*, 1016–1021. [[CrossRef](#)]
40. He, R.; Kyu, T. Effect of plasticization on ionic conductivity enhancement in relation to glass transition temperature of crosslinked polymer electrolyte membranes. *Macromolecules* **2016**, *49*, 5637–5648. [[CrossRef](#)]
41. Fu, G.; Kyu, T. Effect of side-chain branching on enhancement of ionic conductivity and capacity retention of a solid copolymer electrolyte membrane. *Langmuir* **2017**, *33*, 13973–13981. [[CrossRef](#)]
42. Das, S.; Ghosh, A. Ion conduction and relaxation in PEO-LiTFSI- $\text{Al}_2\text{O}_3$  polymer nanocomposite electrolytes. *J. Appl. Phys.* **2015**, *117*, 174103. [[CrossRef](#)]